Materials Horizons

ROYAL SOCIETY OF CHEMISTRY

COMMUNICATION

View Article Online
View Journal | View Issue

Cite this: *Mater. Horiz.*, 2023, **10**, 5223

Received 15th August 2023,
Accepted 11th September 2023

DOI: 10.1039/d3mh01293j

rsc.li/materials-horizons

Dynamic covalent polymer engineering for stable and self-healing perovskite solar cells†

Peng Xu,‡[ab] Jian Liu,‡[a] Shuai Wang,[b] Jiujiang Chen,[a] Bin Han,[a] Yuanyuan Meng,[a] Shuncheng Yang,[a] Lisha Xie,[ac] Mengjin Yang, *[ac] Runping Jia *[b] and Ziyi Ge *[ac]

Perovskite films are susceptible to degradation during their service period due to their weak mechanical properties. Acylhydrazone-bonded waterborne polyurethane (Ab-WPU) was employed as dynamic covalent polymer engineering to develop self-healing perovskite solar cells (SHPSCs). Ab-WPU enhances the crystallinity of the perovskite film, passivates the defects of the perovskite film through functional groups, and demonstrates promising flexibility and mild temperature self-healing properties of SHPSCs. The champion efficiency of SHPSCs on rigid and flexible substrates reaches 24.2% and 21.27% respectively. The moisture and heat stability of devices were improved. After 1000 bending cycles, the Ab-WPU-modified flexible device can be restored to an efficiency of over 95% of its original efficiency by heating to 60 °C. This is because the dynamic acylhydrazone bond can be activated to repair perovskite film defects at a mild temperature of 60 °C as evidenced by *in situ* AFM studies. This strategy provides an effective pathway for dynamic self-healing materials in PSCs under operational conditions.

New concepts

The key contributions of our study are as follows: (1) for the first time, Acylhydrazone-bonded waterborne polyurethane (Ab-WPU) has been introduced into perovskite solar cells, resulting in significantly improved mechanical and thermal stability. (2) Unlike traditional self-healing polymers (mostly with disulfide bonds) used in perovskite solar cells, which require a high activation temperature of 80 °C, Ab-WPU/perovskite exhibits a reduced self-healing temperature of 60 °C, which is the typical temperature when solar cells are under continuous illumination. The reduction of activation temperature enables critical self-healing under normal operation conditions. (3) *In situ* AFM (atomic force microscopy) demonstrated that cracks in Ab-WPU/perovskite were effectively repaired with a simple 60 °C heating process, which justifies that flexible perovskite solar cell's efficiency can be restored to 95% of its original efficiency using the same low thermal treatment. (4) Ab-WPU stands out due to its small and uniform particles, as well as its multifunctional carbonyl groups, which contribute to achieving the highest efficiency (24.2%) among polyurethane-based perovskite solar cells.

1. Introduction

In order to promote the commercialization of perovskite solar cells (PSCs), numerous research groups are committed to achieving devices with outstanding power conversion efficiency (PCE) and long-term stability.[1–9] Inverted (p–i–n) perovskite solar cells have become a hot research field due to their unique interface structure which brings better long-term stability. Recently the certified PCE of p–i–n PSC has reached 25.39% through the efforts of research communities.[10] Developing PSCs that can withstand external stressors for long periods of time remains a challenge despite efforts put into achieving excellent PCE.[11–14] In addition to efficiency and stability, mechanical integrity or mechanics-coupled stability of perovskite solar cells is crucial due to the soft and fragile nature of the perovskite film and ubiquitous mechanical scenarios from fabrication to deployment[15,16] To date, various strategies have been explored to stabilize the lattice of PSCs, such as employing additive engineering and interface modulation engineering. However, these approaches predominantly emphasize the enhancement of perovskite thin film stability by passivating non-radiative recombination defects present at grain boundaries and interfaces of the perovskite.[17–19] Consequently, developing a comprehensive method that simultaneously passivates non-radiative recombination defects in perovskites for improved

[a] *Zhejiang Provincial Engineering Research Center of Energy Optoelectronic Materials and Devices, Ningbo Institute of Materials Technology and Engineering, Chinese Academy of Sciences, Ningbo 315201, P. R. China. E-mail: yangmengjin@nimte.ac.cn, geziyi@nimte.ac.cn*

[b] *School of Materials Science and Engineering, Shanghai Institute of Technology, Shanghai 201418, P. R. China. E-mail: jiarp@sit.edu.cn*

[c] *Center of Materials Science and Optoelectronics Engineering, University of Chinese Academy of Sciences, Beijing, 100049, P. R. China*

† Electronic supplementary information (ESI) available. See DOI: https://doi.org/10.1039/d3mh01293j

‡ Equal contribution.

PSC efficiency, stabilizes the perovskite lattice against temperature and humidity-induced degradation, and repairs defects generated during operation and is of paramount importance.[20,21]

Recently, self-healing materials have been proved to be feasible in repairing crystal defects of perovskite solar cells and restoring device performance.[22] At the same time, self-healing polyurethane as a self-healing material has been successfully introduced into PSCs from many groups.[23–25] However, some reports mentioned that the low electron mobility of self-healing materials will lead to energy disorder in the system, and its addition amount needs to be strictly controlled.[26] This limits the application of self-healing polyurethane in PSCs to some extent. Polyurethane materials can also be divided into several types, such as thermoplastic polyurethane (TPU) and waterborne polyurethane (WPU). In contrast to TPU, WPU incorporates an anionic hydrophilic chain extender with carboxyl groups in the soft segment, which facilitates its smooth dispersion in water. After synthesis, it can maintain a small, uniform particle size in water, which allows for precise control of its addition amount during PSC fabrication.[27] Simultaneously our previous work has proved that the introduction of anionic groups can act on the anionic defects between grain boundaries, reduce the defect density to a certain extent, and improve the efficiency and stability of devices.[28] At present, a disulfide bond is a widely utilized self-healing dynamic bond, with an activation reaction temperature of approximately 65 °C.[29] Typically, when applied as a self-repairing bond within materials, the disulfide bond requires higher temperatures to achieve rapid healing.[30] During the normal deployment of PSCs, the temperature is typically maintained at 50–60 °C through continuous illumination.[31] We developed a self-healing WPU that employs hydrazone bonds to address aforementioned disparities. Under mild stimulation, acylhydrazone bonds can undergo a dynamic reversible reaction at low temperature. Meanwhile the WPU with a very small particle size can be easily dispensed in DMF, allowing it to be successfully introduced into the perovskite system.[32,33]

In this work, a novel self-healing acylhydrazone-bonded waterborne polyurethane (Ab-WPU) with an acylhydrazone bond is employed as a dynamic covalent polymer engineering for perovskites for the first time. By implementing this approach, the unique chemical bonding of the WPU successfully binds to the chalcogenide defects, achieving passivation of defects.[34–36] Moreover, the crystal growth process of perovskite thin films is regulated, and the grain size and crystallinity are increased. Therefore, the Ab-WPU additive increases the PCE of conventional PSCs from 22.28% to 24.2% and the PCE of flexible PSCs from 19.92% to 21.27%. Through the moisture and thermal stability test, it shows excellent hydrothermal stability. In addition, Ab-WPU shows excellent flexibility, which provides good bending resistance for flexible PSCs. More importantly, the dynamic acylhydrazone bond can repair perovskite crystal cracks at 60 °C, and make Ab-WPU customized devices recover more than 95% efficiency by heating after 1000 bends, which helps in the application of self-healing materials to the industrialization of PSCs.

2. Experimental sections

Materials

Solvents. *N*,*N*-Dimethylformamide (DMF, Sigma Aldrich, 99.8%), dimethylsulfoxide (DMSO, Sigma-Aldrich, 99.8%), isopropanol (IPA, General-Reagent, 99.7%), ethanol (General-Reagent, 99.5%), and chlorobenzene (CB, Sigma Aldrich, 99.8%) were used as solvents.

Reagents. Formamidinium iodide (FAI, Advanced Election Technology Co, Ltd, 99.99%), lead(II) iodide (PbI_2, Advanced Election Technology Co, Ltd, 99.99%), lead(II) bromine ($PbBr_2$, Advanced Election Technology CO, Ltd, 99.999%), [6,6]-phenyl-C61-butyric acid methyl ester ($PC_{61}BM$, Lumtec, 99%), bathocuproine (BCP, Advanced Election Technology Co, Ltd, 99.9%), [2-(3,6-dimethoxy-9*H*-carbazol-9-yl)ethyl]phosphonic acid (MeO-2PACz, TCI, 98.0%), poly(3-(4-carboxybutyl)thiophene) (P3CT, Rieke Metals, 99%), and sodium hydroxide (NaOH, Polymer Light Technology Inc. Co, Ltd, 99.99%) were used.

Ab-WPU synthesis

First, 6 g of PBA, 10.97 g of IPDI, 1.187 g of DMPA and a trace amount of DBTDL were loaded into a four-necked flask equipped with a nitrogen inlet, a condenser, and a stirrer, and the reaction was carried out for 2–3 hours at 85 °C under a N_2 atmosphere. The temperature of the flask was then cooled to 60 °C and 0.696 g of BDO and 0.199 g of PA were added to the flask as chain extender and the reaction was continued for another 1.5 h. After adjusting the reaction temperature to 40 °C, the prepolymer was neutralized with 0.895 g of TEA and reacted for about 30 minutes. Finally, 50 mL of deionized water was added to the prepolymer and stirred at 1000 rpm for 10 min to obtain the final Ab-WPU. The synthesized Ab-WPU had a molar ratio of 1.2 between NCO groups and OH groups. Subsequently, DMF was further added to make the desired concentration.

Preparation of precursor solution

Preparation of the perovskite precursor: FAI (301 mg), PbI_2 (806.8 mg), $PbBr_2$ (91.8 mg), and CsBr (53.2 mg) were added to a 1.2 mL DMF and DMSO mixed solvent (DMF: DMSO = 7 : 1 volume ratio) to formulate a perovskite precursor solution. It was stirred for 5 hours with a magnetic stirrer to fully dissolve salts. The prepared perovskite precursor solution was divided it into three parts, and Ab-WPU solutions were added to achieve 2.5, 5, and 10 mg mL^{-1} Ab WPU concentrations.

Preparation of SAM (MeO-2PACz) solution: 0.6 mg of MeO-2PACz was added to 2 mL of anhydrous ethanol solvent.

Preparation of the P3CT-Na precursor. Poly(3-(4-carboxybutyl)thiophene) (P3CT) and sodium hydroxide (NaOH) were mixed in deionized water to form P3CT-Na. 9 mg of P3CT and 1.975 mg of NaOH were first dissolved in 5.5 mL of deionized water. In order to improve the solubility of the P3CT polymer in water, 550 μL of DMF was added and subjected to 30 minutes of ultrasonic treatment. NaOH/aqueous solution was slowly added to a deep purple P3CT/aqueous solution to reduce the thermal effect of heat release. The ratio of water to DMF is 10 : 1.

The solution was stirred at 40 °C for 6 hours to prepare the P3CT–Na polymer.

Preparation of $PC_{61}BM$ solution. 25 Mg of $PC_{61}BM$ was added to 1 mL chlorobenzene solvent, and the solution was stirred to fully dissolve PC61BM.

Preparation of BCP solution. 15 Mg of BCP was added to 3 ml isopropanol solvent.

Preparation of Ab-WPU modified perovskite solar cells

FTO glass with 15 Ω sq^{-1} resistance and 85% transmittance was ordered from Youxuan Tech. FTO was cleaned twice with ultrasonic cleaning in deionized water, acetone, and IPA. The substrate was transferred into a glove box after 5 min of plasma treatment. 50 μL of the MeO-2PACz precursor solution was added onto the FTO substrate, spin-coated at 3000 rpm for 30 seconds, followed by 100 °C annealing for 10 minutes. Next, the perovskite film was formed by spin-coating 50 μL of the precursor at 4000 rpm for 25 seconds, and 350 μL diethyl ether was dropped onto the substrate in the last 10 seconds. Perovskite film was further annealed at 100 °C for 60 minutes. 50 μL of the $PC_{61}BM$ electron transport layer precursor was spin coated onto the perovskite absorbing layer, rotated at a speed of 2000 rpm for 30 seconds, and annealed at 70 °C for 60 seconds to obtain an electron transport layer. 100 μL of the BCP passivation layer precursor was spun onto the electron transport layer, rotated at 4000 rpm for 30 seconds, and then annealed at 100 °C for 60 seconds to obtain the passivation layer. Finally, the prepared sample was placed in a vacuum evaporation coating equipment. After reaching a vacuum of 1×10^{-4} Pa, an Ag electrode coating with a thickness of 80 nm was deposited at an evaporation rate of 0.01 nm s^{-1}, and the effective area of the device was 0.04 cm^2.

Preparation of flexible Ab-WPU-modified perovskite solar cells

Etched PEN/ITO substrates were placed in distilled water for ultrasonic cleaning for 30 minutes, and then transferred into a mixture of detergent and distilled water for ultrasonic cleaning for 30 minutes. The above steps were repeated three times. Subsequently, isopropanol ultrasonic cleaning was conducted three times. Finally, ether ultrasonic cleaning was used 3 times, each time lasting 30 minutes. The cleaned PEN/ITO substrates were dried with N_2 and treated with plasma for five minutes. Other processes were identical to those used with rigid FTO substrates in the previous text.

Thermal stability test and the preparation of perovskite solar cells

Preparation of P3CT-Na hole transport layer: the P3CT-Na precursor solution, which had been prepared, was taken in an amount of 100 μL and dropped onto the substrate. Then, we spin coated it at a speed of 6000 rpm for 30 seconds, deposited an ultra-thin layer of P3CT-Na, and annealed it at 120 °C P3CT-Na, then other processes were carried out consistent with the previous preparation method.

Experimental characterization

The *J–V* curves of PSCs were measured at room temperature in a nitrogen environment. The light source parameters are 450 W xenon lamp (Newport riel Sol3A), the digital source meter is Keithley 2400, and calibrated to 100 mW cm^{-2} using a silicon reference cell AK-200 (Konica Minolta). We chose a scanning rate between 0.01 and 0.5 V s^{-1} for the measurement; IPCE records the incident photon to current conversion efficiency (IPCE) spectrum using a Keithley 2400 light source meter and an Oriel Cornerstone $260\frac{1}{4}$ m monochromator under a 300 W xenon lamp illumination. And we quantified the monochromatic photon flux using a calibrated silicon cell method. The photovoltaic performance of cell devices needs to be mutually proven using the photovoltaic parameters of the *J–V* curve and the integrated current results of IPCE testing; the morphology of perovskite films was characterized using a scanning electron microscope (Verios G4 UC, USA), with a practical acceleration voltage of 2 kV; the FTO/perovskite was characterized using a PL mapping tester (China PMEye-3000), and the sample was excited using a 450 nm laser in this experiment. The femtosecond transient absorption TA spectrum was measured using a Newport's SOL-35F-1K-HP-T under a 400 nm excitation light source. Using an X-ray diffractometer (XRD) (German ADVANCE D8), the scanning range of the perovskite is found to be 5–60°, and the scanning rate is 6° min^{-1}. The FTIR spectrum was detected by FTIR-840S (Shimadzu) and XPS/UPS analysis was performed using an AXIS Ultra DLD spectrometer (Cretos Analytics, UK) and monochromatic Al K, respectively, an α X-ray source (1486.6 eV) and a He discharge lamp (21.22 eV of He I radiation). The XPS measurement spectrum is obtained using a hemispherical analyzer set to 160 eV through energy, while high-resolution narrow scanning is performed using 40 eV through energy. A dimension Icon (Veeco) was used for conducting atomic force microscopy (c-AFM) in air. A constant external bias voltage of −1.0 V and a platinum coated conductive probe were used for the measurement. The humidity stability test of PSC devices was conducted by placing them in a sealed environment with saturated KCl solution at room temperature (where the hygrometer indicated approximately 85% humidity). After a set period of storage, these devices were transferred to a glove box for efficiency testing. Similarly we placed the device on a calibrated 85 °C hot plate and stored it for thermal stability in an environment filled with N_2.

3. Results and discussion

First, we designed an acylated perylene glycol (PA) as a chain extender for WPUs and synthesized self-healing waterborne polyurethanes (Ab-WPU) from PA, PBA, IPDI, BDO, and DMPA. The detailed synthesis process is shown in Fig. S1 (ESI†). The presence of PA peaks at 1617.43 cm^{-1} and 1599.37 cm^{-1} was observed through infrared absorption (FTIR) spectrogram S2, indicating the successful introduction of acylhydrazone glycol into WPU. The synthesized Ab-WPU has a smaller dispersion particle size, and the particle size of the polymer solution is less

than 100 nm.[37] Next, we conducted thermogravimetric analysis (TGA) to test the thermal stability of Ab-WPU. As shown in Fig. S3 (ESI†), the high-temperature decomposition temperature above 250 °C indicates that it has excellent thermal stability. Due to its large molecular weight, Ab-WPU does not easily enter the perovskite lattice. Instead, it resides at the grain boundaries, where it regulates and controls the crystallization process and passivates charge defects.[23] In addition, a smaller particle size can mitigate the impact of polyurethane addition on device efficiency. Subsequent tests have shown that it will not form a thicker, non-conductive polymer film that would hinder carrier transport within 10 mg mL^{-1} concentration.

In our study, we modified perovskite film with 5 mg mL^{-1} Ab-WPU and conducted a series of subsequent experiments. Firstly, the surface morphology of the perovskite light-absorbing layer was investigated through scanning electron microscopy (SEM). Fig. 1a, b, c and d are the top view and cross-section scanning electron microscopy images of the perovskite film. The highly crystalline and more uniform perovskite film with a large grain size was obtained by spin-coating the mixed solution of Ab-WPU and the perovskite precursor on the FTO substrate. The film thickness remained unchanged. To further verify the effect of Ab-WPU on the crystal structure, X-ray diffraction (XRD) analysis was performed on perovskite thin films added with Ab-WPU and control devices. As shown in Fig. 1e and Fig. S16 (ESI†), the crystal structure of the perovskite film after Ab-WPU passivation treatment is not different from that of the perovskite film without Ab-WPU treatment. The FWHM of the device XRD curves for the control and Ab-WPU were calculated to be 0.175 and 0.16, so the diffraction peak of the perovskite film after Ab-WPU treatment becomes stronger and sharper than that of the original film, which indicates that its crystallinity is enhanced and the grain size is increased. SEM and XRD analysis results clearly show that the Ab-WPU additive has a significant positive impact on crystallization behavior. In addition, after Ab-WPU treatment, the α-phase perovskite diffraction peak increases, but does not convert to additional δ-phase perovskite, while the diffraction peak of residual PbI_2 at 12.8° did not increase, even some decreased, indicating that Ab-WPU has a potential passivation defect effect. Therefore, Ab-WPU additive may be used as a Pb atom chelating agent to delay the crystallization rate of the perovskite,[38] which is conducive to the formation of large and uniform perovskite films. This enhanced crystallinity is conducive to improving device efficiency. Polyurethane, as a polymer, can be used as an additive to regulate the GBs of the perovskite, change the surface uniformity of perovskite films, promote the nucleation and crystallization of perovskite, and contribute to improving the performance and stability of PSCs.[38,39]

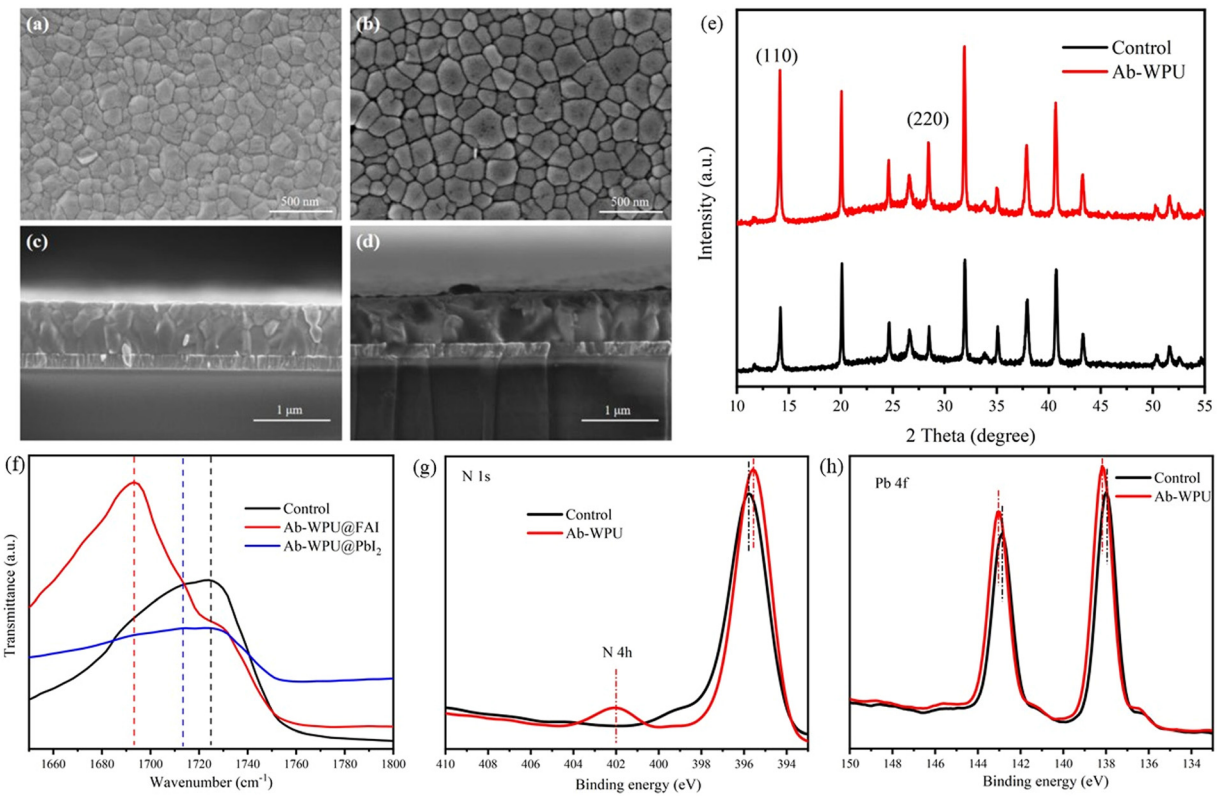

Fig. 1 (a) and (c) The top view and cross-section view SEM images of the perovskite film without Ab-WPU modification. (b) and (d) The top view and cross-section view SEM images of the perovskite film with Ab-WPU modification. (e) The XRD images of the perovskite layer without Ab-WPU modification and with Ab WPU modification. (f) The FTIR comparison between Ab-WPU and Ab-WPU combined with FAI or PbI_2 and (g) and (h) XPS comparison of perovskite layer without Ab-WPU modification and with Ab-WPU modification.

In order to verify the interaction between Ab-WPU charge distribution and perovskite defects, as shown in Fig. S6 and S7 (ESI†), we split Ab-WPU into three structural units and conducted DFT calculations. The C═O of these structural units has strong electronegativity, which makes it easier to be approached by uncoordinated Pb^{2+}. At the same time, compared with C═O on the whole polymer chain, side chain carboxyl of WPU without CH_2 hindrance is more effective in binding defects. And we also conducted Fourier transform infrared spectroscopy (FTIR) to investigate the interaction of C═O bonds with defects such as FA^+ and Pb^{2+} in Ab-WPU (Fig. 1f). It is observed from the spectra that the C═O peak at 1725 cm^{-1} of polyurethane shifts in the direction of enhanced binding energy after the combination of PbI_2, FAI and Ab-WPU, which implies that the anion-defective vacancies can be bound to C═O for passivation modification of the chalcogenide film.[40] In order to further investigate the passivation sites, we conducted X-ray photoelectron spectroscopy (XPS) measurements. Fig. S8, S19 (ESI†) and Fig. 1g, h show the effect of Ab-WPU on the perovskite. The appearance of the peak value of *N* 4 h at 402 cm^{-1} proves the introduction of additives. Compared with the control sample, the diffraction peaks of N 1s and O 1s of the Ab-WPU-treated perovskite films were shifted to the direction of low binding energy, which proved that the bonds in Ab-WPU were coordinated with the ions in the perovskite. And due to this interaction the peaks corresponding to I 3d and Pb 4f simultaneously shifted toward the high value of the binding energy.[23,39,41] In summary, it has been proven that the structure of Ab-WPU has been successfully modified in perovskite and has played a good passivation effect on defects.

Next, we performed steady-state photoluminescence (PL) spectroscopy and time-resolved photoluminescence (TRPL) studies to assess the impact of Ab-WPU on charge carrier dynamics at the interface of $FA_{0.87}Cs_{0.13}PbI_{2.7}Br_{0.3}$. Both Ab-WPU passivated and untreated perovskite thin films were fabricated on FTO glass substrates. As depicted in Fig. 2a, the emission peak intensity of the perovskite film following Ab-WPU passivation is considerably augmented, suggesting a reduction in surface defects and enhanced crystallinity of the modified film.[25] The figure also presents the recovery kinetics of transient bleaching signals detected at 752 nm in the transient absorption (TA) spectra of both the reference and Ab-WPU modified perovskite films.[42–44] Fig. S9 (ESI†) illustrates the origin of the TA bleaching signal at 752 nm in the perovskite film, which stems from the band edge state filling of photoexcited charge carriers. The recovery kinetics can be indicative of the charge carrier recombination process. Notably, none of the investigated samples exhibited ultrafast decay in their TA kinetics, implying that the deposition of Ab-WPU did not introduce any rapid decay pathways for charge carriers in the perovskite. However, the TA of the polymer-treated film exhibited slower carrier decay as compared to the control sample (Fig. 2c).[34] This observation is further substantiated by the TRPL spectra of the two types of perovskite thin films investigated. As illustrated in Fig. 2b, the Ab-WPU doped perovskite film exhibits prolonged PL decay in comparison to the pristine film. The lifetimes of perovskite films with Ab-WPU addition are τ_1 = 45.44 ns, τ_2 = 184.82 ns, and τ_{Avg} = 99.8 ns, whereas those of the pristine film are τ_1 = 37.52 ns, τ_2 = 154.26 ns, and τ_{Avg} = 66.71 ns. These findings indicate lower defect concentration and superior electronic quality in the

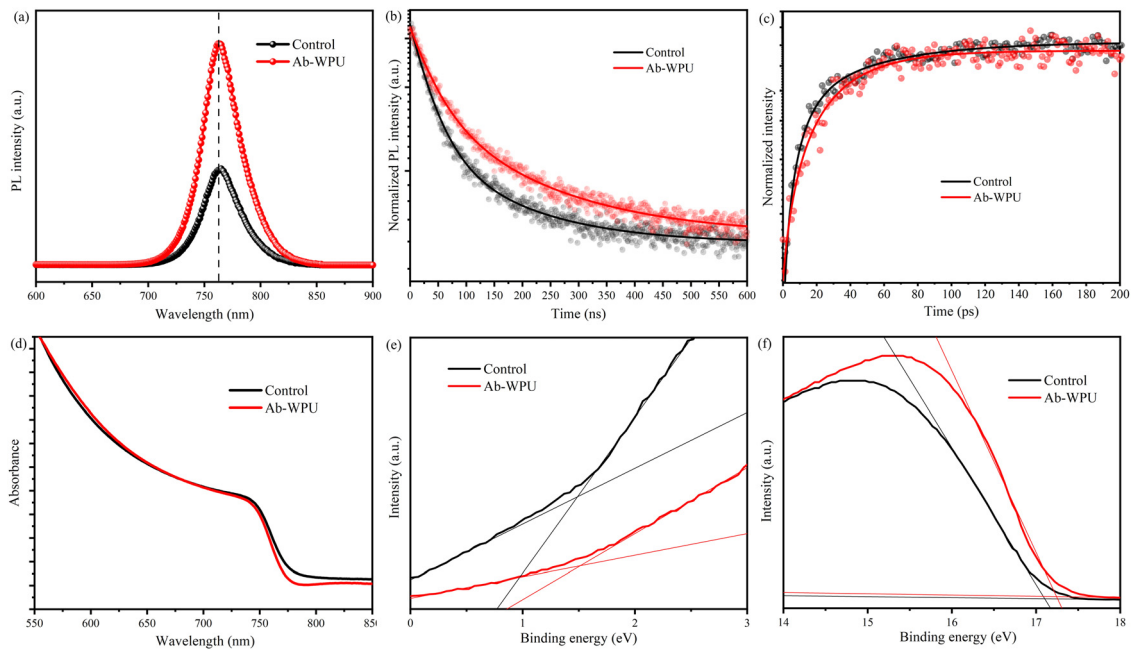

Fig. 2 Perovskite film without additives and modified by AB-WPU (a) PL spectrum, (b) time resolved photoluminescence (TRPL) spectrum, (c) transient absorption (TA) decay curve, (d) ultraviolet visible absorption (UV) spectrum and (e) and (f) ultraviolet photoelectron spectroscopy (UPS).

Ab-WPU-incorporated perovskite film, which implies that the Ab-WPU modified devices are likely to exhibit high open-circuit voltage (V_{OC}) and fill factor (FF).

To verify the compatibility of energy levels between the Ab-WPU modified perovskite functional layer and other functional layers in the PSC devices, we performed ultraviolet photoemission spectroscopy (UPS) and ultraviolet-visible spectroscopy (UV-vis) tests. Fig. 2d displays the UV-vis spectra, showing relatively low values below 800 nm and an overall stable trend. This is in agreement with the SEM analysis mentioned earlier, which confirms the flatness of the film. We then constructed a Tauc plot (Fig. S10, ESI†) based on the UV-vis spectra, which revealed a similar bandgap after modification as per the direct bandgap formula $(\alpha Hv)^2 = A(hv - E_g)$. Then, we characterized the surface electronic structure of the perovskite thin films using UPS, as presented in Fig. 2e and f. The work function (WF) was determined by the secondary electron cutoff region, which decreased from 4.12 eV to 3.97 eV upon the addition of Ab-WPU. Moreover, the Fermi level (EF) position relative to the maximum valence band (VBM) shifted from 1.49 eV to 1.52 eV, indicating that Ab-WPU covered the perovskite, promoting the formation of a more n-type perovskite surface, which is well-matched with the upper electron transport layer.[45]

To further investigate the influence of Ab-WPU incorporation on the performance of PSC devices, we constructed an inverted perovskite solar cell structure with FTO/MeO-2PACz/Ab-WPU@$FA_{0.87}Cs_{0.13}PbI_{2.7}Br_{0.3}$/$PC_{61}BM$/BCP/Ag, as shown in Fig. 3a. Utilizing the calculated HOMO and LUMO energy levels, the energy level distribution diagram of PSC devices was plotted. As shown in Fig. 3b, more n-type perovskites can further improve the electron extraction efficiency of the perovskite/top electron transport layer interface. Moreover, as the VB declines, the energy level of perovskite becomes more compatible with the hole transport layer, aiding in the reduction of energy loss at the MeO-2PACz/perovskite interface layer. This, in turn, leads to an augmented V_{OC} in the modified device.[46]

Next, we fabricated three different concentrations of Ab-WPU modified PSC devices, as illustrated in Fig. 3c and Fig. S11 (ESI†). The photovoltaic performance parameters of 10 devices

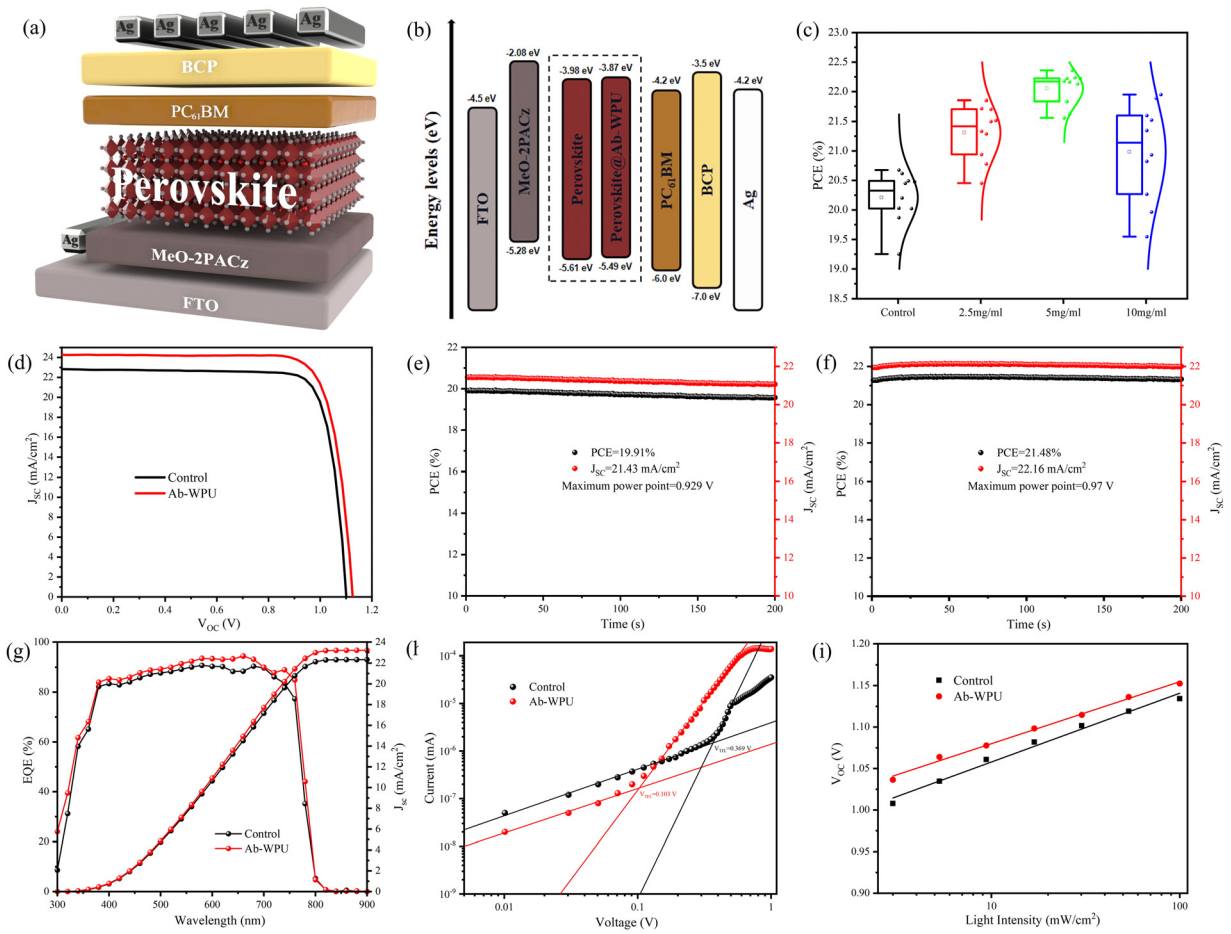

Fig. 3 (a) Structure diagram of the inverted perovskite solar cell, (b) energy level diagram of the perovskite solar cell without additives and modified by Ab-WPU, (c) PCE statistics of 10 different batches of solar cells prepared before and after PSC treatment with different concentrations of Ab WPU, (d) *J*–*V* curve of the best device of perovskite solar cell without additives and modified by Ab-WPU, (e) and (f) MPP stable power output, (g) EQE spectrum and integrated current density, (h) *J*–*V* characteristic curve of electronic transmission devices (FTO/$PC_{61}BM$/Perovskite/$PC_{61}BM$/Ag) and (i) comparison of the light intensity dependence of the standard and Ab-WPU doped PSCs.

with varying concentrations were evaluated, including photovoltaic conversion efficiency (PCE), open-circuit voltage (V_{OC}), short-circuit current density (J_{SC}), and fill factor (FF). Of all devices tested, those modified with 5 mg mL^{-1} of Ab-WPU had the highest PCE. The photoluminescence (PL) test revealed that perovskite thin films containing Ab-WPU demonstrated good passivation. A high concentration of self-healing additives also contributes to improving the self-healing ability of the perovskite thin film. But Fig. 3c shows that due to the insulating nature of Ab-WPU, PCE and J_{SC} values progressively decrease with increasing concentration, and excessive doping leads to instability in both V_{OC} and FF. The optimized *J–V* curve for the reference device and the Ab-WPU modified device is presented in Fig. 3d, and the photovoltaic parameters are summarized in Table S1 (ESI†). The PCE value of the reference device is 20.49%, the J_{SC} value is 23.22 mA cm^{-2}, the V_{OC} value is 1.13 V, and the FF is 78.06%. But the PCE value of the Ab-WPU modified device noticeably increased from 20.49% to 22.43%, accompanied by a V_{OC} value of 1.152 V, a J_{SC} value of 23.88 mA cm^{-2}, and a FF value of 81.5%. As previously mentioned, high crystallinity is advantageous for achieving high V_{OC} and FF in the corresponding devices. Furthermore, the smaller particle size distribution of the polymer results in a relatively low molecular weight, while the modified perovskite crystal exhibits higher crystallinity and a more uniform surface, ensuring efficient charge transfer. Consequently, the device's current density does not significantly decrease with the increasing amount of Ab-WPU added. The incident photon-to-current conversion efficiency (IPCE) curve demonstrates that compared to the control device, the Ab-WPU modified device exhibits enhanced light-harvesting capability, which can be ascribed to reduced defects. The current density aligns with the *J–V* curve (Fig. 3g). Simultaneously, we monitored the steady-state photocurrent output of the device within 200 s at the maximum power point (Fig. 3e and f) to assess the device's stable power output. Upon applying a bias voltage of 0.97 V to the Ab-WPU modified device, we observed a stable J_{SC} value of 22.16 mA cm^{-2} and a PCE of 21.48%, while the reference device exhibited a stable J_{SC} of 21.4 mA cm^{-2} and a PCE of 19.91% when a bias voltage of 0.929 V was applied. Moreover, the steady-state test of the Ab-WPU modified device displayed better stability over 200 s. Through Fig. S16 and S17 (ESI†), we find a slight hysteresis effect in both devices through the forward and reverse scanning results of the control and Ab-WPU devices.

Quantitative evaluation of defects in perovskite thin films was performed using space-charge-limited-current (SCLC) measurements. A device consisting solely of an electron transport layer was fabricated, with a structure of FTO/$PC_{61}BM$/perovskite/$PC_{61}BM$/Ag. As depicted in Fig. 3h, the curve satisfies n_1 = 1; $n_2 > 3$; a sudden increase in current beyond the inflection point implies that the injected carriers occupy the defects. The trap-filled limit voltage (V_{tfl}) of the SHPSC device is 0.103 V, while the V_{tfl} of the reference device is 0.369 V. The defect density (n_t) can be calculated using the formula $n_t = 2\varepsilon\varepsilon_0 V_{tfl}/ed^2$ (ε_0 is the vacuum dielectric constant, ε is the relative dielectric constant, e is the elemental charge, and d is the film thickness). Using this formula, the defect densities for the reference and SHPSC devices were found to be 1.452×10^{14} cm^{-3} and 4.053×10^{13} cm^{-3}, respectively. The reduction in defect density confirms that Ab-WPU successfully passivated defects in the perovskite films, which is in agreement with the PL results.[47]

We performed light intensity dependent measurements on the PSC devices before and after modification, and the intensity dependence of the V_{OC} further demonstrated enhanced charge transfer in the perovskite film upon the addition of Ab-WPU. The relationship between V_{OC} and light intensity exhibits slopes of 1.386 K_bT/q (PSCs) and 1.208 K_bT/q (SHPSCs), as illustrated in Fig. 3i. The slope is derived from the formula $V_{OC} = [(s \times K_bT)/q] \times \ln(P_{light})$, where K_b is the Boltzmann constant, T is the temperature, and q is the elementary charge. The findings suggest that the defects in the SHPSC devices are fewer than those in the PSC devices, and the non-radiative composite is suppressed, which is in strong agreement with other experimental results.

To further verify the universality of self-healing waterborne polyurethane (Ab-WPU) as an additive for enhancing the efficiency of perovskite solar cells (PSCs), we investigated the impact of Ab-WPU on the $FA_{0.96}Cs_{0.04}PbI_{2.8}Br_{0.12}$ perovskite. We prepared inverted PSCs with the structure FTO/MeO-2PACz/$FA_{0.96}Cs_{0.04}PbI_{2.8}Br_{0.12}$ (Ab-WPU)/C_{60}/BCP/Ag. This system contained a lower concentration of Cs^+ compared to previous devices, making it closer to a pure FA system with a narrower bandgap, resulting in higher J_{SC}. The original device exhibited a PCE of 22.28%, with a J_{SC} value of 25.26 mA cm^{-2}, a V_{OC} value

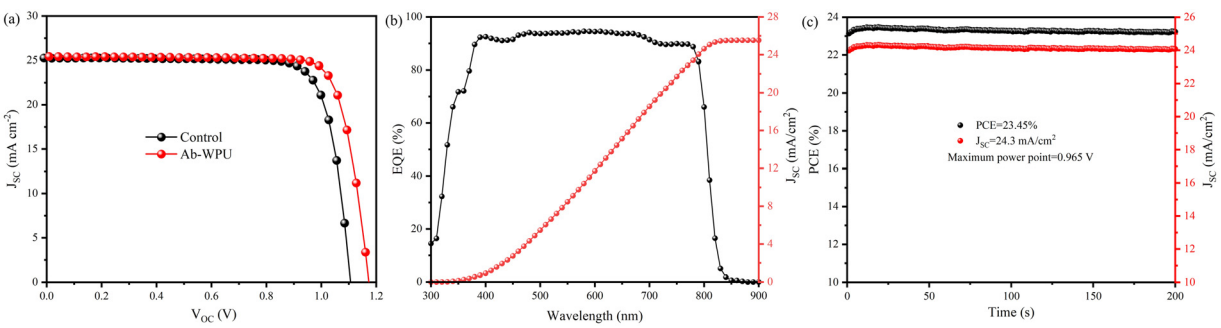

Fig. 4 (a) *J–V* curve of the best device of perovskite solar cell without additives and modified by AB-WPU, (b) EQE spectrum and integrated current density, and (c) MPP stable power output.

of 1.104 V, and an FF value of 79.89%. After modification with 5 mg mL^{-1} Ab-WPU, the device showed a significant improvement in the PCE of 24.2%, with a J_{SC} value of 25.41 mA cm^{-2}, V_{OC} value of 1.172 V, and a high fill factor (FF) of 81.26% (Fig. 4a). According to our examination of several polyurethane-modified PSC devices, as depicted in Table S2 (ESI†), our WPU modified devices demonstrate higher PCE compared to conventional TPU devices. The integrated current density from EQE testing matched well with J_{sc} from the J–V curves (Fig. 4b). The statistical analysis of PCE distribution from 15 points confirmed the reproducibility of these devices (Fig. S15, ESI†). Furthermore, the stable PCE output matched well with the J–V measurement at the MPP within 200 s (Fig. 4c).

Subsequently, to further explore the practical impact of self-healing performance on PSCs, we fabricated flexible PSC devices using polyethylene naphthalate (PEN) as a substrate. Fig. 5a presents the schematic diagram and J–V curve of the flexible device. Upon the addition of Ab-WPU modification, the device efficiency increased from 19.22% to 21.27%, a V_{OC} value from 1.097 V to 1.141 V, a J_{SC} value from 22.9 mA cm^{-2} to 23.25 mA cm^{-2}, and FF values from 76.48% to 80.21%. The device parameters of the modified SHPSC devices have significantly improved. Table S5 (ESI†) illustrates that our work achieves impressive efficiency for flexible devices, with a reduced performance gap between rigid and flexible devices following the Ab-WPU modification. The next step involves evaluating the self-healing performance of SHPSCs, given that multiple bending cycles can induce irreversible damage and considerably limit their practical application. Thus, we verified the self-repairing mechanism of SHPSCs through thermal heating. We then bent a cylinder with a diameter of 6 mm in a glove box and recorded the efficiency loss at 100, 400, 700, 1000, 1100, 1400, 1700, and 2000 bending. During this process, the device was heated on a 60 °C hotplate for 30 minutes when the bending reached 1000 and 2000 cycles. As depicted in Fig. 5b, the introduction of polymers led to virtually no efficiency loss at the beginning. However, as the number of bending cycles increased, more crack defects appeared in the flexible devices, and the efficiency loss became more evident. At 1000 cycles, the efficiency decreased to 82%. Nevertheless, after heat treatment for 30 minutes at 60 °C, the efficiency recovered to 96%, exhibiting significant recovery effects. However, after 400 additional bending cycles, the defects recoverable by the water-based polyurethane bond reappeared alongside other potential defects, resulting in a substantial efficiency reduction. Overall, after 2000 bending cycles, the efficiency decreased to 73%, but following reheating treatment, and the efficiency could still be restored to 80%. This result demonstrates that the introduction of self-healing waterborne polyurethane can heal defects caused by device bending and restore efficiency. To further corroborate the self-healing of membrane layers, atomic force microscopy (AFM) was employed to characterize the self-healing process, as depicted in Fig. 5c. The perovskite thin film displays evident cracks after multiple bending cycles, with fractures occurring along the grain boundary. Intriguingly, following the self-healing process of thermal annealing (60 °C, 10 min), the cracks in the perovskite thin film vanish, and healing traces manifest at the former cracks. Under the influence of temperature and lone pair electrons in the perovskite, the acylhydrazone is

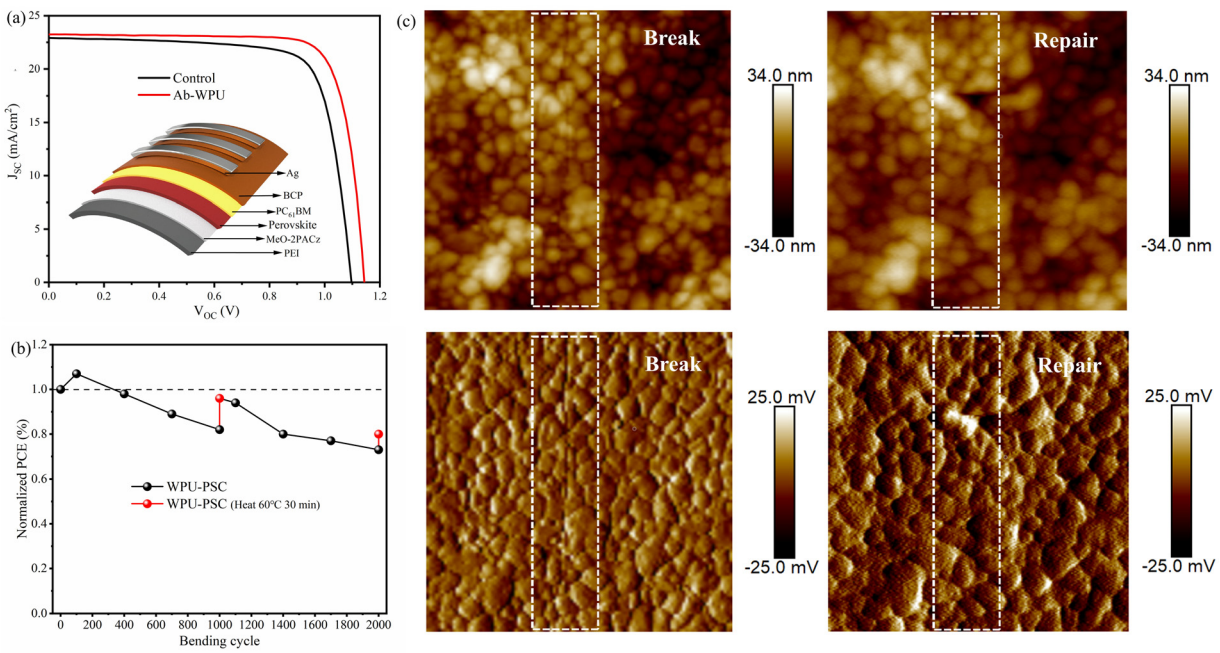

Fig. 5 (a) Structure diagram and J–V curve of flexible perovskite solar cells without additives and modified with AB-WPU. (b) Bending resistance test of flexible perovskite solar cell devices treated with AB-WPU and efficiency test of device self-healing by heating at 1000 and 2000 bending cycles, respectively. (c) AFM images of cracks in perovskite films before and after self-healing (left and right).

stimulated, and the dynamic bond undergoes a reduction reaction to mend the fracture.

To further investigate how Ab-WPU can enable PSCs to develop self-healing ability, we first tested and characterized the self-healing performance of Ab-WPU. The polymer solution of Ab-WPU was poured into the mold and dried at 100 °C in an oven to obtain the polymer model shown in Fig. 6b. Then we cut the model from the middle as shown in Fig. 6b, and then heated it on a hot bench to 60 °C. The broken model was tightly pressed together, and we added a few drops of acetic acid solution at the fracture site. We found that it only took 10 minutes for the model to heal. According to literature research, a schematic diagram of the self-healing process is shown in Fig. 6a.[48] After the fracture of the sample, the acylhydrazone and H bonds on the fracture surface were destroyed. When the fracture surface is in close contact and stimulated by acid and heat, acylhydrazone bonds and H bonds can be reconstructed to achieve self-healing of polymer materials. We attempted to replace acid stimulation with PbI_2 dissolved in DMF and found that it can also achieve Ab-WPU healing as shown in Fig. S4 (ESI†). Further research was conducted on the self-healing mechanism of Ab-WPU@perovskite thin film, and Fig. 6c depicts its self-healing process mechanism. During the use of PSCs, they absorb heat from sunlight. Ab-WPU, which is bound between perovskite grain boundaries or overlies perovskite, softens due to its viscoelasticity, which is easier to absorb stress than crystals and causes bending and fracture (Fig. S5, ESI†). However, when the heat is absorbed to a certain extent, the fracture surface is cracked into acylhydrazone groups of free aldehydes and hydrazine. Under the stimulation of free Pb^{2+} and I^- conditions in perovskite films, the crack surface heals, two acylhydrazone groups undergo the reversible metathesis

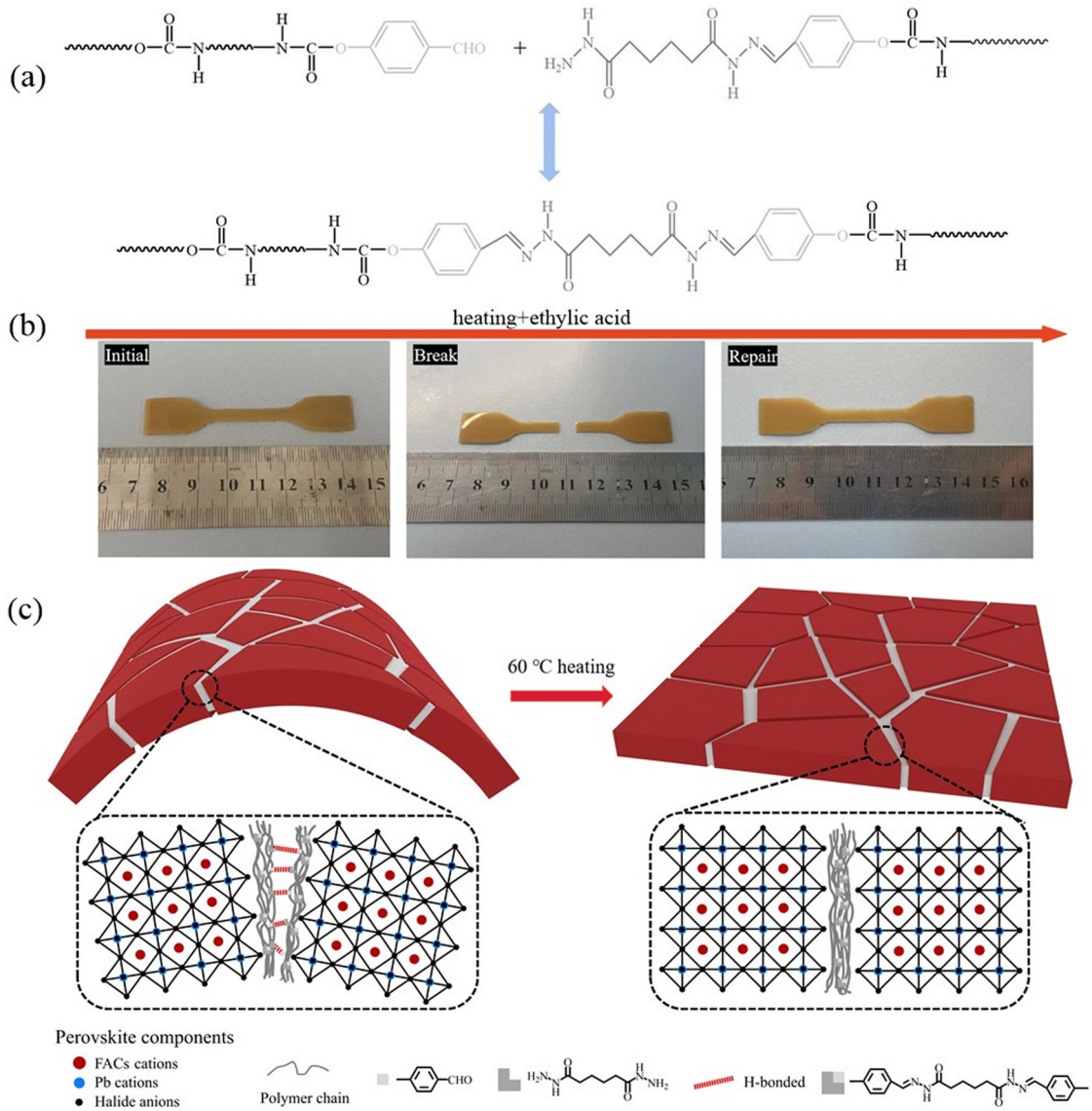

Fig. 6 (a) Schematic diagram of the Ab-WPU self-healing process, (b) Ab-WPU like self-healing experiment, and the (c) mechanism of Ab-WPU@perovskite membrane self-healing.

reaction. In addition, hydrogen bonding plays an auxiliary role in crack repair. This low-temperature self-healing method is more suitable for passivation modification of perovskite solar cells that will not be used under high temperature conditions compared to disulfide bond healing. When Ab-WPU participates in the passivation of the perovskite layer, it successfully distributes to the grain boundaries and interfaces of the perovskite, achieving passivation of charge defects, enhancing thermal stability, reducing water erosion, and increasing self-healing performance.

Finally, we test the stability of PSCs. The storage stability of PSC devices with Ab-WPU on a rigid substrate was first tested in a glove box. We tracked the efficiency of these devices stored in an N_2 environment for different time periods. As shown in Fig. S14 (ESI†), after 2800 h of storage, the device retains 90% of the initial PCE value, indicating that these devices have good storage stability. To further explore the stability of the device in an 85% humidity environment, the device was stored in a saturated KCl solution in a sealed environment. As shown in Fig. 7a, we can see that the humidity resistance of the device modified by Ab-WPU is significantly improved. We conducted water contact angle tests on the comparison device, the device modified by Ab-WPU, and Ab-WPU to explore the reasons for the improved moisture resistance. The results (Fig. S12, ESI†) showed that the water contact angle of the device with Ab-WPU added was similar to that of the device without Ab-WPU and larger than that of the pure perovskite film, which indicated that a Ab-WPU layer was formed on the perovskite film. This hydrophobic film slows down the erosion of the perovskite by water.

To test the existence of excellent thermal stability of SHPSC devices at self-healing temperatures, we also measured the storage stability at 60 °C in a N_2 environment. Some studies have reported that MeO-2PACz exhibits poor heat resistance.[49,50] As a result, we constructed an inverted perovskite solar cell structure comprising FTO/P3CT-Na/Ab-WPU@$FA_{0.87}Cs_{0.13}PbI_{2.7}Br_{0.3}$/$PC_{61}BM$/BCP/Ag to investigate the thermal stability of SHPSCs. Fig. S13 (ESI†) displays the *J*–*V* curve of this structure, while the device parameters are presented in Table S4 (ESI†). The PCE of the Ab-WPU modified device

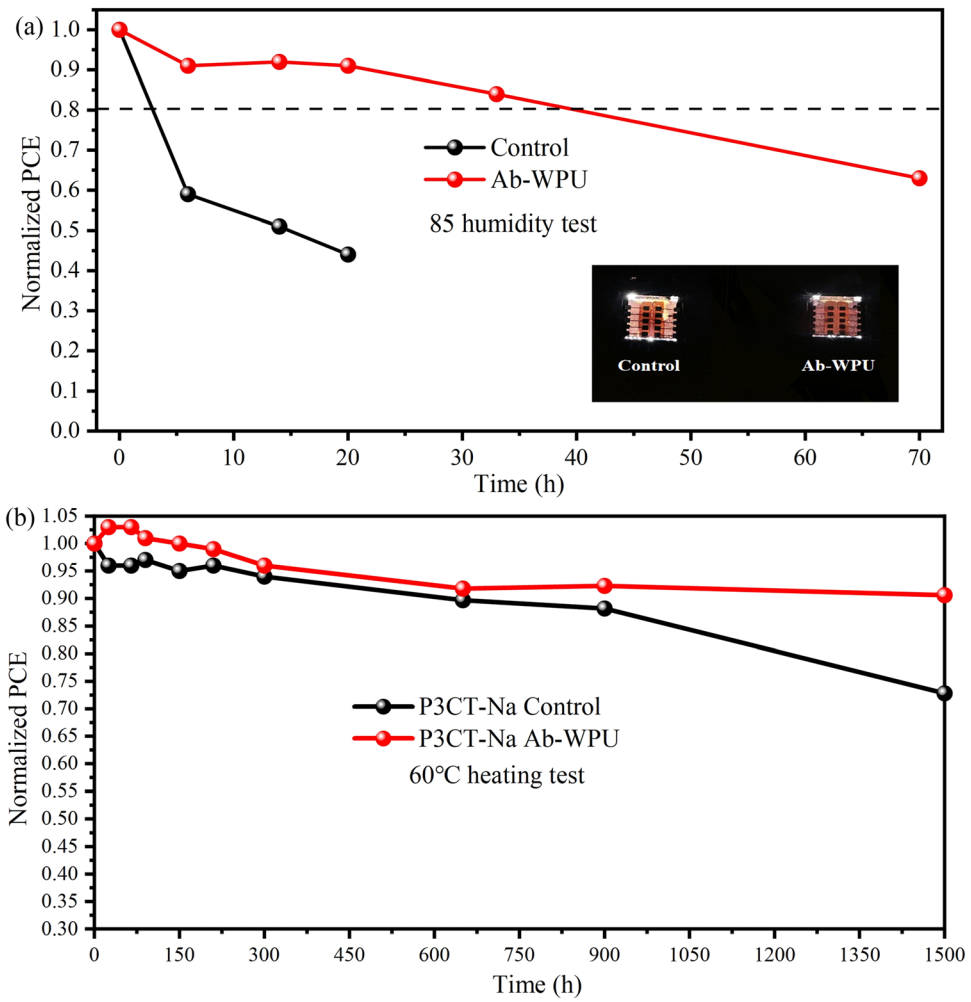

Fig. 7 (a) Normalized PCE plots of PSC devices without additives and modified with AB-WPU, stored in an 85% humidity environment (b) normalized PCE plots of PSC devices without additives and modified with AB-WPU, stored in an N_2 environment at 60 °C.

increased from 20.45% to 21.88%. Fig. 7b reveals that, under heating conditions, the initial decline rate of the untreated device and the efficiency of the device with the addition of Ab-WPU additives remain relatively stable, maintaining over 95%. Following more than 300 h of heat testing, all devices exhibited a downward trend. When the heating duration surpasses 600 h, the efficiency loss rate of the standard piece notably exceeds that of SHPSCs. The stability during the initial 300 hours indicates that the perovskite in the FAC system possesses a certain degree of stability at 60 °C. The phenomenon observed after 300 h may be attributed to defect passivation and the thermal insulation effect of the polymer. This confirms that Ab-WPU has successfully achieved a thermal insulation effect, reducing the temperature impact on device efficiency. Simultaneously, the passivation of defects also enhances the thermal stability of PSCs to a certain extent.

4. Conclusions

In summary, we introduce Ab-WPU into perovskite membranes to achieve self-healing of SHPSCs, improve efficiency, and enhance device stability, especially thermal stability. Ab-WPU passivates surface defects through the binding between carbonyl (CO) or carboxyl (COOH) and Pb^{2+}, achieving grain boundary regulation and defect management, to some extent reducing water and temperature effects. Importantly, under the stimulation of temperature and lone pair electrons, Ab-WPU with acylhydrazone bonds is activated and exchanged, thereby achieving self-healing flexible perovskite solar cells after cracking. A champion efficiency of 24.2% was achieved on the rigid substrate. Therefore, after thermal annealing at 60 °C, it also maintained an efficiency of over 90% of the initial power conversion efficiency. This method introduces water-based polyurethane into PSCs for the first time, demonstrating a simple method for manufacturing efficient self-healing SHPSCs, which provides an effective strategy for extending the lifespan of perovskite photovoltaics and improving their competitiveness.

Author contributions

P. X. and M. Y. conceived and designed the experiments; P. X. and J. L. fabricated devices. S. W. and R. J. synthesized Ab-WPU. J. C., B. H. and L. X. assisted in SEM, UPS, SCLC, and contact angle measurements. Y. M. performed TA measurements. S. Y. conducted charge distribution calculations. M. Y. and Z. G. supervised the projects and finalized the manuscript. P. X. wrote the first draft, and all authors gave comments during the revision.

Conflicts of interest

Patent covering the Ab-WPU for self-healing perovskite solar cells has been filed by authors' institution.

Acknowledgements

P. X., J. L., J. C., and M. Y. acknowledge the funding from the Ningbo Institute of Materials and Technology CAS and the Ningbo Yongjiang Talent Introduction Programme (2022A-009-C). P. X., S. W. and R. J. acknowledge the funding from the Natural Science Foundation of Shanghai (19ZR1455000) and the Shanghai Sailing Program (21YF1446800 and 22YF1447900). L. J., B. H., J. C., Y. M., S. Y., L. X. M. Y. and Z. G. are supported by the National Natural Science Foundation of China (U21A20331, 81903743 and 62275251), the National Science Foundation for Distinguished Young Scholars (21925506) and the Natural Science Foundation of Ningbo (2021J192).

References

1 A. Kojima, K. Teshima, Y. Shirai and T. Miyasaka, *J. Am. Chem. Soc.*, 2009, **131**, 6050–6051.
2 S. He, L. Qiu, L. K. Ono and Y. Qi, *Mater. Sci. Eng., R*, 2020, **140**, 100545.
3 M. M. Lee, J. Teuscher, T. Miyasaka, T. N. Murakami and H. J. Snaith, *Science*, 2012, **338**, 643–647.
4 T. Leijtens, R. Prasanna, K. A. Bush, G. E. Eperon, J. A. Raiford, A. Gold-Parker, E. J. Wolf, S. A. Swifter, C. C. Boyd and H.-P. Wang, *Sustainable Energy Fuels*, 2018, **2**, 2450–2459.
5 S. Akin, *ACS Appl. Mater. Interfaces*, 2019, **11**, 39998–40005.
6 H. Zhou, Q. Chen, G. Li, S. Luo, T. Song, H.-S. Duan, Z. Hong, J. You, Y. Liu and Y. Yang, *Science*, 2014, **345**, 542–546.
7 W. Chen, Y. Zhou, G. Chen, Y. Wu, B. Tu, F.-Z. Liu, L. Huang, A. M. C. Ng, A. B. Djurišić and Z. He, *Adv. Energy Mater.*, 2019, **9**, 1803872.
8 J. Song, L. Zhao, S. Huang, X. Yan, Q. Qiu, Y. Zhao, L. Zhu, Y. Qiang, H. Li and G. Li, *ChemSusChem*, 2021, **14**, 1396–1403.
9 H. Min, D. Y. Lee, J. Kim, G. Kim, K. S. Lee, J. Kim, M. J. Paik, Y. K. Kim, K. S. Kim and M. G. Kim, *Nature*, 2021, **598**, 444–450.
10 Q. Tan, Z. Li, G. Luo, X. Zhang, B. Che, G. Chen, H. Gao, D. He, G. Ma and J. Wang, *Nature*, 2023, 1–3.
11 Q. Zhou, Y. Gao, C. Cai, Z. Zhang, J. Xu, Z. Yuan and P. Gao, *Angew. Chem., Int. Ed.*, 2021, **60**, 8303–8312.
12 M. Abdi-Jalebi, Z. Andaji-Garmaroudi, S. Cacovich, C. Stavrakas, B. Philippe, J. M. Richter, M. Alsari, E. P. Booker, E. M. Hutter and A. J. Pearson, *Nature*, 2018, **555**, 497–501.
13 J. Tong, Z. Song, D. H. Kim, X. Chen, C. Chen, A. F. Palmstrom, P. F. Ndione, M. O. Reese, S. P. Dunfield and O. G. Reid, *Science*, 2019, **364**, 475–479.
14 G. Nazir, S.-Y. Lee, J.-H. Lee, A. Rehman, J.-K. Lee, S. I. Seok and S.-J. Park, *Adv. Mater.*, 2022, **34**, 2204380.
15 N. Rolston, B. L. Watson, C. D. Bailie, M. D. McGehee, J. P. Bastos, R. Gehlhaar, J.-E. Kim, D. Vak, A. T. Mallajosyula and G. Gupta, *Extreme Mech. Lett.*, 2016, **9**, 353–358.
16 Q. Tu, D. Kim, M. Shyikh and M. G. Kanatzidis, *Matter*, 2021, **4**, 2765–2809.

17 F. Gao, Y. Zhao, X. Zhang and J. You, *Adv. Energy Mater.*, 2020, **10**, 1902650.
18 X. Guo, N. Li, Y. Xu, J. Zhao, F. Cui, Y. Chen, X. Du, Q. Song, G. Zhang and X. Cheng, *Adv. Funct. Mater.*, 2023, 2213995.
19 N. Li, A. Feng, X. Guo, J. Wu, S. Xie, Q. Lin, X. Jiang, Y. Liu, Z. Chen and X. Tao, *Adv. Energy Mater.*, 2022, **12**, 2103241.
20 X. Hu, X. Meng, L. Zhang, Y. Zhang, Z. Cai, Z. Huang, M. Su, Y. Wang, M. Li and F. Li, *Joule*, 2019, **3**, 2205–2218.
21 B. J. Worfolk, S. C. Andrews, S. Park, J. Reinspach, N. Liu, M. F. Toney, S. C. Mannsfeld and Z. Bao, *Proc. Natl. Acad. Sci. U. S. A.*, 2015, **112**, 14138–14143.
22 C. Ge, X. Liu, Z. Yang, H. Li, W. Niu, X. Liu and Q. Dong, *Angew. Chem., Int. Ed.*, 2022, **61**, e202116602.
23 T. Zheng, Q. Zhou, T. Yang, Y. Zhao, B. Fan, J. Bo, L. Fan and R. Peng, *Carbon*, 2022, **196**, 213–219.
24 T. Xue, Z. Huang, P. Zhang, M. Su, X. Hu, T. Wu, B. Fan, G. Chen, G. Yu and W. Liu, *InfoMat*, 2022, **4**, e12358.
25 Q. Zhang, J. Duan, Q. Guo, J. Zhang, D. Zheng, F. Yi, X. Yang, Y. Duan and Q. Tang, *Angew. Chem., Int. Ed.*, 2022, **61**, e202116632.
26 X. Meng, Z. Xing, X. Hu, Z. Huang, T. Hu, L. Tan, F. Li and Y. Chen, *Angew. Chem., Int. Ed.*, 2020, **59**, 16602–16608.
27 P. Si and B. Zhao, *Can. J. Chem. Eng.*, 2021, **99**, 1851–1869.
28 P. Xu, L. Xie, S. Yang, B. Han, J. Liu, J. Chen, C. Liu, R. Jia, M. Yang and Z. Ge, *Solar RRL*, 2023, **7**, 2200858.
29 Y. Xu and D. Chen, *Macromol. Chem. Phys.*, 2016, **217**, 1191–1196.
30 D.-I. Lee, S.-H. Kim and D.-S. Lee, *Molecules*, 2019, **24**, 1492.
31 X. Luo, X. Lin, F. Gao, Y. Zhao, X. Li, L. Zhan, Z. Qiu, J. Wang, C. Chen and L. Meng, *Sci. China Chem.*, 2022, 1–48.
32 G. Deng, F. Li, H. Yu, F. Liu, C. Liu, W. Sun, H. Jiang and Y. Chen, Dynamic hydrogels with an environmental adaptive self-healing ability and dual responsive sol–gel transitions, *ACS Macro Lett. 1*, 2012, **1**, 275–279.
33 X. Yang, G. Liu, L. Peng, J. Guo, L. Tao, J. Yuan, C. Chang, Y. Wei and L. Zhang, *Adv. Funct. Mater.*, 2017, **27**, 1703174.
34 M. Wang, Y. Zhao, X. Jiang, Y. Yin, I. Yavuz, P. Zhu, A. Zhang, G. S. Han, H. S. Jung and Y. Zhou, *Joule*, 2022, **6**, 1032–1048.
35 F. Tan, H. Tan, M. I. Saidaminov, M. Wei, M. Liu, A. Mei, P. Li, B. Zhang, C.-S. Tan and X. Gong, *Adv. Mater.*, 2019, **31**, 1807435.
36 P. Ferdowsi, E. Ochoa-Martinez, S. S. Alonso, U. Steiner and M. Saliba, *Sci. Rep.*, 2020, **10**, 1–10.
37 J. Ren, X. Dong, Y. Duan, L. Lin, X. Xu, J. Shi, R. Jia, D. Wu and X. He, *J. Appl. Polym. Sci.*, 2022, **139**, 52144.
38 Z. Huang, X. Hu, C. Liu, L. Tan and Y. Chen, *Adv. Funct. Mater.*, 2017, **27**, 1703061.
39 Y. Lan, Y. Wang, Y. Lai, Z. Cai, M. Tao, Y. Wang, M. Li, X. Dong and Y. Song, *Nano Energy*, 2022, **100**, 107523.
40 T.-H. Han, J.-W. Lee, C. Choi, S. Tan, C. Lee, Y. Zhao, Z. Dai, N. De Marco, S.-J. Lee and S.-H. Bae, *Nat. Commun.*, 2019, **10**, 520.
41 Y. Guo, S. Apergi, N. Li, M. Chen, C. Yin, Z. Yuan, F. Gao, F. Xie, G. Brocks and S. Tao, *Nat. Commun.*, 2021, **12**, 644.
42 M. Salado, M. Andresini, P. Huang, M. T. Khan, F. Ciriaco, S. Kazim and S. Ahmad, *Adv. Funct. Mater.*, 2020, **30**, 1910561.
43 L. Xie, J. Liu, J. Li, C. Liu, Z. Pu, P. Xu, Y. Wang, Y. Meng, M. Yang and Z. Ge, *Adv. Mater.*, 2023, 2302752.
44 Z. Yin, J. Leng, S. Wang, G. Liang, W. Tian, K. Wu and S. Jin, *J. Am. Chem. Soc.*, 2021, **143**, 4725–4731.
45 W. Dong, W. Qiao, S. Xiong, J. Yang, X. Wang, L. Ding, Y. Yao and Q. Bao, *Nano-Micro Lett.*, 2022, **14**, 1–11.
46 L. Zhang, K. Cao, J. Qian, Y. Huang, X. Wang, M. Ge, W. Shen, F. Huang, M. Wang and W. Zhang, *J. Mater. Chem. C*, 2020, **8**, 17482–17490.
47 S. Wang, Z. Li, Y. Zhang, X. Liu, J. Han, X. Li, Z. Liu, S. Liu and W. C. Choy, *Adv. Funct. Mater.*, 2019, **29**, 1900417.
48 G. Deng, C. Tang, F. Li, H. Jiang and Y. Chen, *Macromolecules*, 2010, **43**, 1191–1194.
49 D. Zhang, H. Zhang, H. Guo, F. Ye, S. Liu and Y. Wu, *Adv. Funct. Mater.*, 2022, **32**, 2200174.
50 A. Al-Ashouri, E. Köhnen, B. Li, A. Magomedov, H. Hempel, P. Caprioglio, J. A. Márquez, A. B. Morales Vilches, E. Kasparavicius and J. A. Smith, *Science*, 2020, **370**, 1300–1309.

